Journal of Physical Oceanography

Supporting Information for

A diagnostic framework linking eddy flux ellipse with eddy-mean energy exchange

Yi Yang[1], Ru Chen[1], Glenn R. Flierl[2], and Hong Zhang[3]

[1] School of Marine Science and Technology, Tianjin University, Tianjin, China.

[2] Massachusetts Institute of Technology, Cambridge, Massachusetts, USA.

[3] The University of California, Los Angeles, CA, USA

Corresponding author: Ru Chen (ruchen@alum.mit.edu)

Contents of this file

Text S1. Eddy momentum ellipse and eddy buoyancy ellipse

At any given geographic location, one can infer eddy momentum ellipse using the time series of eddy velocities (u', v') at that location. The derivation of the relation between eddy velocities (u', v') and ellipse properties a_m, b_m and θ_m is shown in Appendix A. Similarly, one can infer eddy buoyancy ellipse using the time series of $(u'_n, \widetilde{b}')$ at any given geographic location. And schematic diagrams of eddy momentum ellipse and eddy buoyancy ellipse are shown in Figure S1.

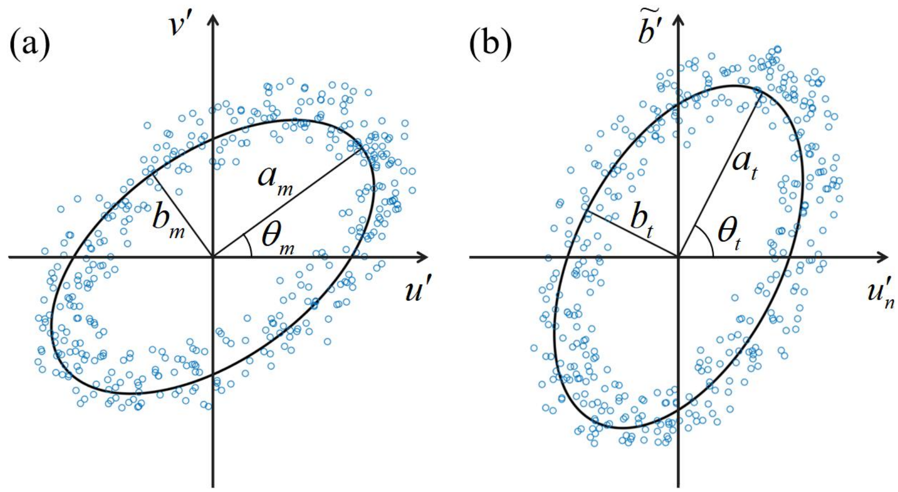

Figure S1. (a) Schematic diagram of eddy momentum ellipse. The scattered dots correspond to the (u', v') time series in the (u', v') space at a selected geographical location. Variables a_m and b_m are the semi-major axis and semi-minor axis of the eddy momentum ellipse, respectively; and θ_m is the angle of eddy momentum ellipse. (b) Schematic diagram of eddy buoyancy ellipse. The scattered dots correspond to the $(u'_n, \widetilde{b}')$ time sercies in the $(u'_n, \widetilde{b}')$ space at a selected geographical location. Variables a_t and b_t are the semi-major axis and semi-minor axis of the eddy buoyancy ellipse, respectively; and θ_t is the angle of eddy buoyancy ellipse.

Text S2. Model-data comparison

Text S2a. Hydrographic variability

To evaluate whether the cube92 version of the ECCO2 state estimate is sufficiently realistic, we carried about the model-data comparison about the hydrographic variability. We compared the hydrographic variability observations from Forget and Wunsch (2007) with the cube92 counterpart. The overall patterns of the temperature variablity from the ECCO2 model are consistent with those from observations (e.g., Figure S2). For example, at 250m, both observed and modeled patterns have elevated values at the western boundary current extensions and the Antarctic Circumpolar Current. The relative difference $|\sigma_{To} - \sigma_{Tm}|/\sigma_{To}$ is less than 0.5 in most regions, and the regions with value more than 0.5 are mainly located at the Southern Ocean and high latitudes.

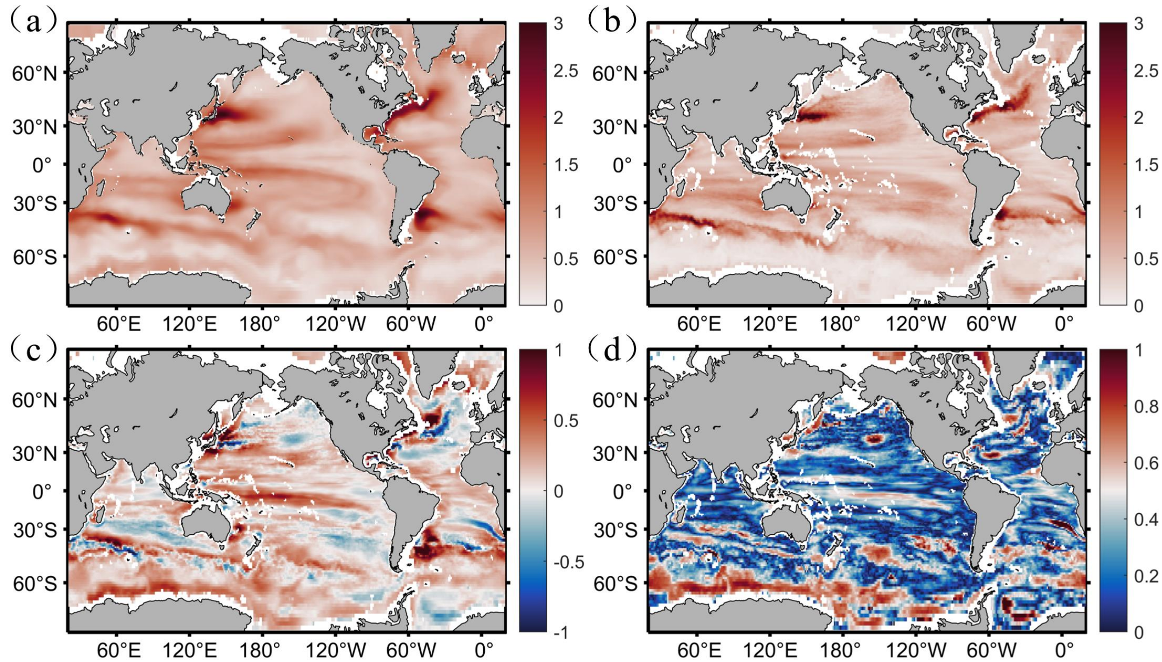

Figure S2. The standard deviation of temperature (℃) at 250m calculated from (a) the hydrographic variability observations in Forget and Wunsch (2007) and (b) the ECCO2 model. They are denoted by σ_{To} and σ_{Tm} respectively. (c) The difference ($\sigma_{To} - \sigma_{Tm}$) (℃) and (d) the relative difference ($|\sigma_{To} - \sigma_{Tm}|/\sigma_{To}$).

Figure S3 shows the zonally averaged relative difference of the temperature/salinity standard deviations between the ECCO2 model and observations. The relative difference is generally small in the upper ocean at mid- and low latitudes. The relative difference of the temperature variability is smaller than that of salinity. These results are consistent with those in Chen (2013), which analyzed the cube87 version of the ECCO2 state estimate.

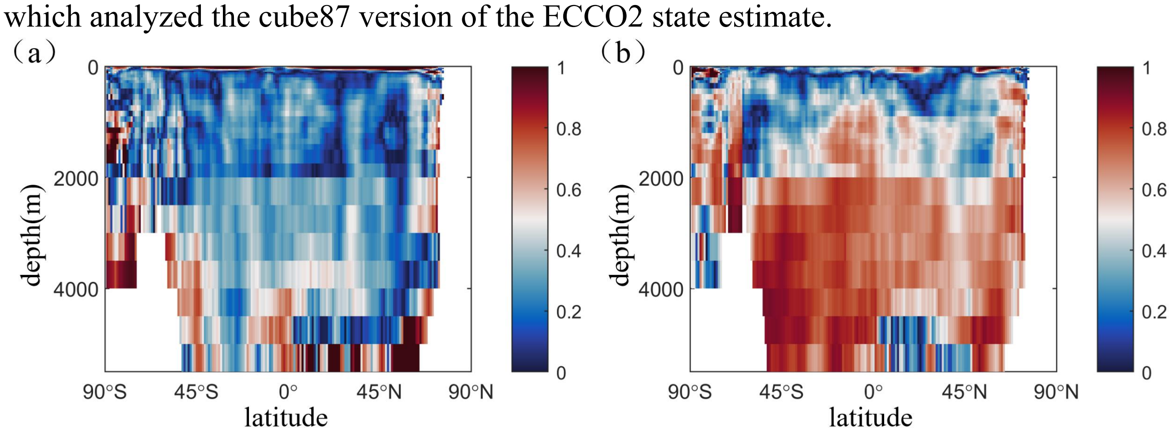

Figure S3. The zonally averaged relative difference between the obervations in Forget and Wunsch (2007) and the ECCO2 state estimate. (a) $|\sigma_{To} - \sigma_{Tm}|/\sigma_{To}$. (b) $|\sigma_{So} - \sigma_{Sm}|/\sigma_{So}$. Here σ_{To} and

σ_{Tm} denote the standard deviation of temperature from observations and the ECCO2 model, respectively. Similary, σ_{S_o} and σ_{S_M} are those for salinity.

Text S2b. Comparison about the M terms

To evaluate whether ECCO2 model reasonably captures the horizontal normal strain and shear strain components of M_{K_E}, we compare these two components with those from AVISO data. The geostrophic contribution to M_{K_E}, M_{NS} and M_{SS} (i.e., $M_{K_{E,G}}$, $M_{NS,G}$ and $M_{SS,G}$) can be estimated from sea surface height [Eqs. (20) and (21)]. Figure S4 shows that $M_{K_{E,G}}$, $M_{NS,G}$ and $M_{SS,G}$ from ECCO2 generally agree with those from AVISO observations. For both ECCO2 and AVISO, large vallues occur at the western boundary currents, its extensions and in the Southern Ocean. However, these terms from ECCO2 are smaller than those from AVISO. Figure S5 shows that for both ECCO2 and AVISO, the zonally averaged $M_{K_{E,G}}$, $M_{NS,G}$ and $M_{SS,G}$ have peaks near 40°S, 10°N, 25°N and 35°N.

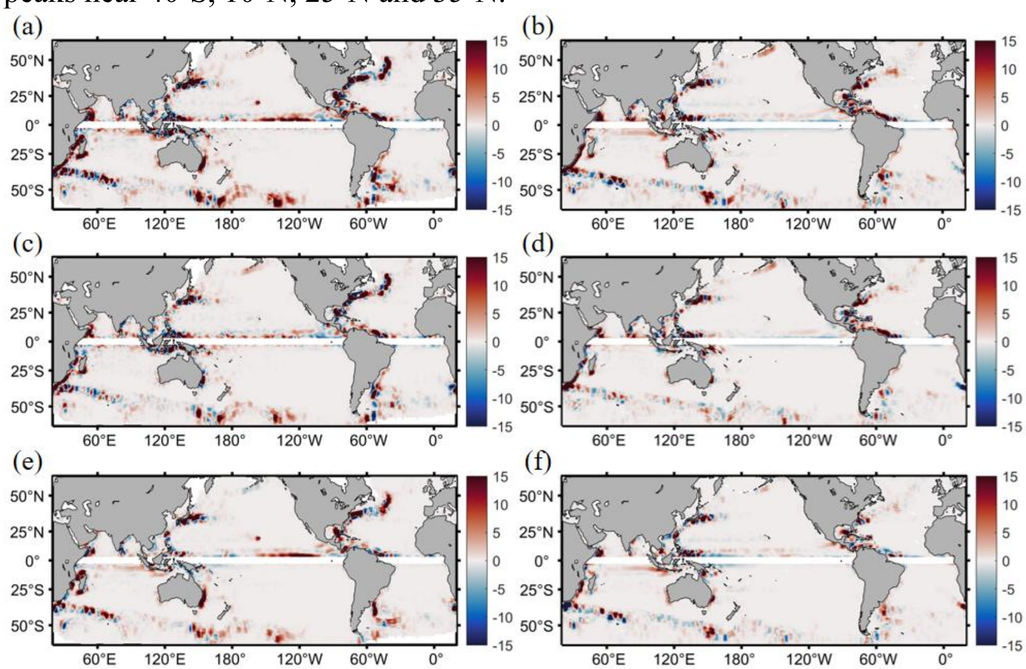

Figure S4. (a) $M_{K_{E,G}}$ [Eq. (20)], (c) $M_{NS,G}$ [Eq. (21)] and (e) $M_{SS,G}$ [Eq. (21)] using the sea surface height data during 1993-2003 from AVISO. (b) $M_{K_{E,G}}$, (d) $M_{NS,G}$ and (f) $M_{SS,G}$ using the sea surface height data during 1993-2003 from ECCO2 model. A 3° running average is applied here. Considering that $M_{K_{E,G}}$, $M_{NS,G}$ and $M_{SS,G}$ breaks down at the equator, regions within 3° of the equator are masked.

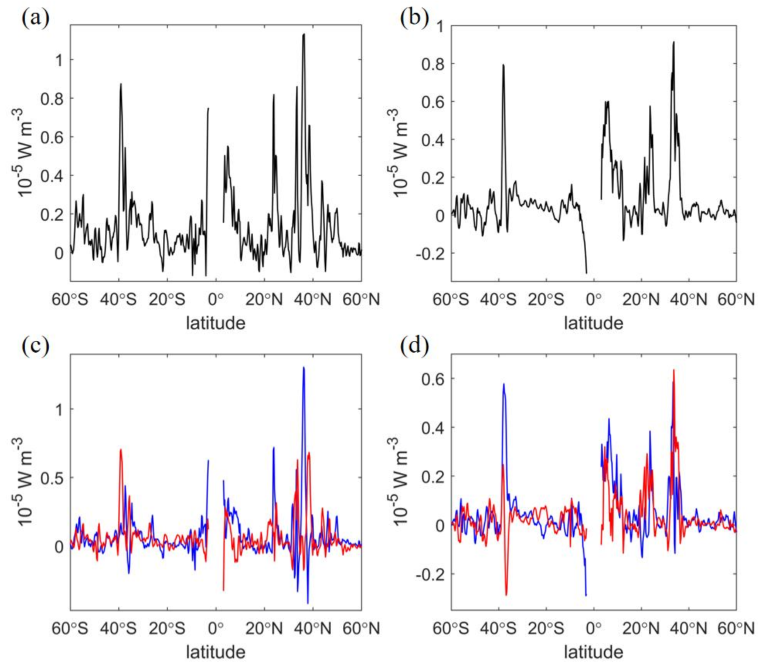

Figure S5. The zonally averaged $M_{K_{E,G}}$ [Eq. (20)] for the years 1993-2003 from (a) AVISO observations and (b) the ECCO2 model. The zonally averaged $M_{NS,G}$ (blue) and $M_{SS,G}$ (red) [Eq. (21)] during 1993-2003 from (c) AVISO observations and (d) the ECCO2 model.

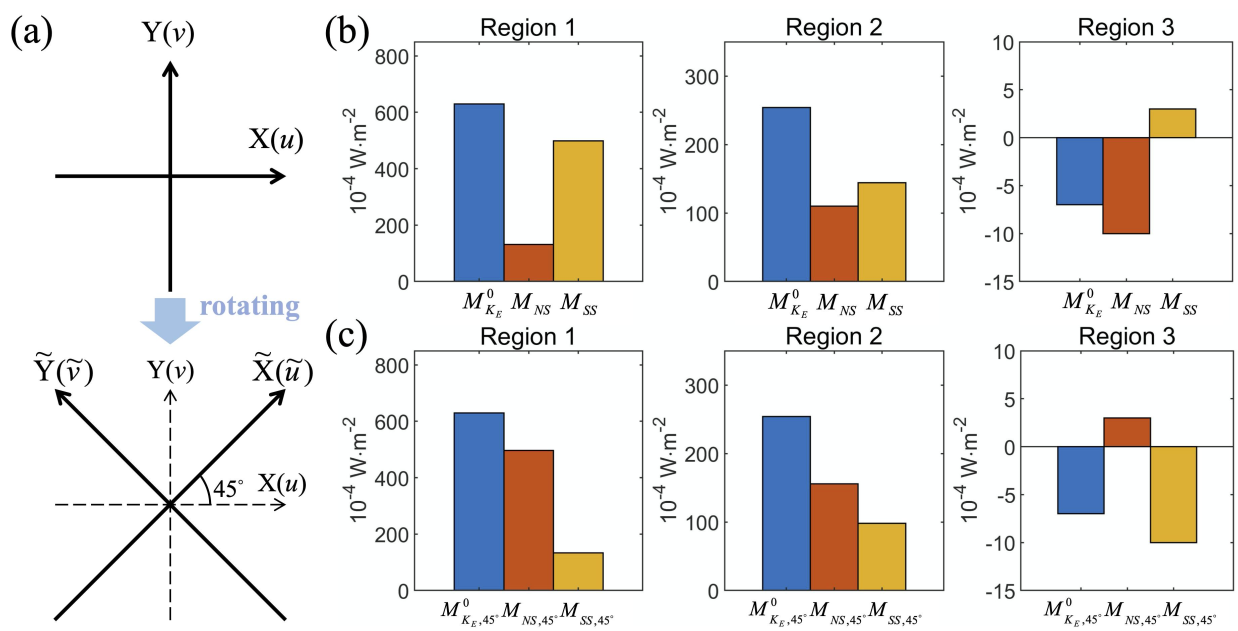

Figure S6. (a) The conventional longitude-latitude coordinate (X,Y) and the new coordinate rotated by 45° ($\tilde{X}$,$\tilde{Y}$). (b) The regionally averaged $M^0_{K_E}$, M_{NS} and M_{ss} in the conventional longitude-latitude coordinate (X,Y) over the upper 30 levels (1106 m) in the three regions shown in Fig. 11a. (c) The same as (b), but for those in the new coordinate ($\tilde{X}$,$\tilde{Y}$), which is rotated from the conventional coordinate by 45^o.

Text S3. Results from MITgcm llc4320 solution

To assess whether results presented in Sections 5a-5c are sensitive to the choice of model resolution, besides the ECCO2 state estimate, we also analyzed the high-resolution MITgcm llc4320 solution. Figure S7 shows the Lorenz diagrams from the MITgcm llc4320 output, which are qualitatively similar to those from ECCO2 (Fig. 9 in the main text). For both solutions, eddies obtain energy from the mean flow in the western part of the Kuroshio Extension and release energy in the east. Figure S8 shows that the ellipse orientation at the ocean surface from MITgcm llc4320. It is similar to that from ECCO2 in the following aspects. The major axis of the ellipse generally leans against the mean flow shear in the western part of the Kuroshio Extension jet (Regions 1 and 2). Compared to Regions 1 and 2, the ellipse orientation is much more meridional in the eastern part of the domain (e.g., Region 3). Figure S9 shows the structures of eddy-mean energy exchange and eddy/mean properties as a function of depth and off-jet distance from MITgcm llc4320. It is nearly similar to its ECCO2 counterpart (Fig. 14 in the main text). For example, for both solutions, the patterns of $\partial \overline{\rho^*}/\partial x_n$ and $EKE_n + EAPE$ well match the D_{P_E} structure in both upstream and downstream of the Kuroshio.

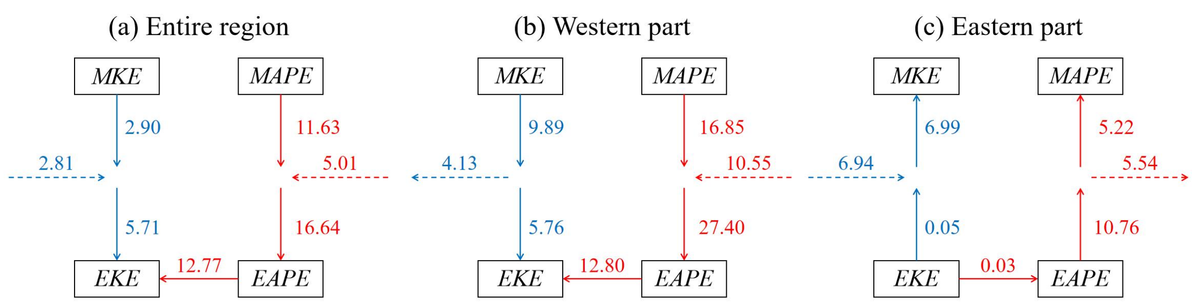

Figure S7. The same as Fig. 9 in the main text, but based on the MITgcm llc4320 solution (2011/09/13-2012/11/14).

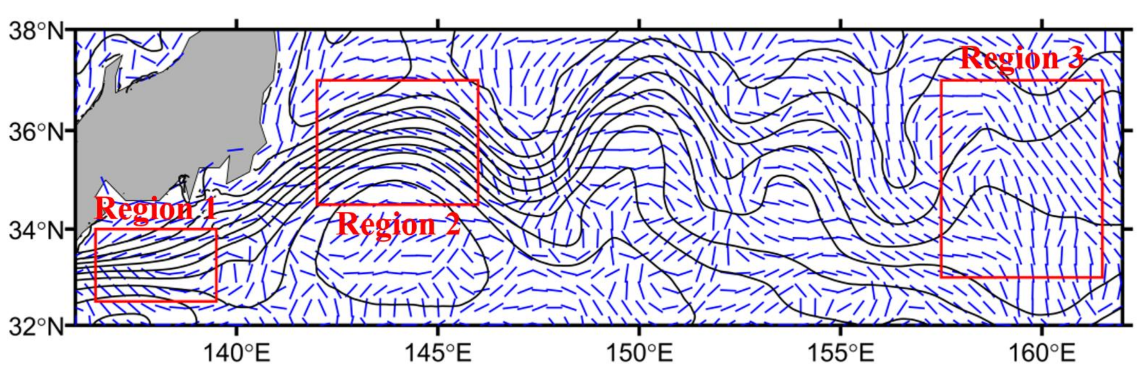

Figure S8. The same as Fig. 12a, but based on the MITgcm llc4320 solution (2011/09/13-2012/11/14).

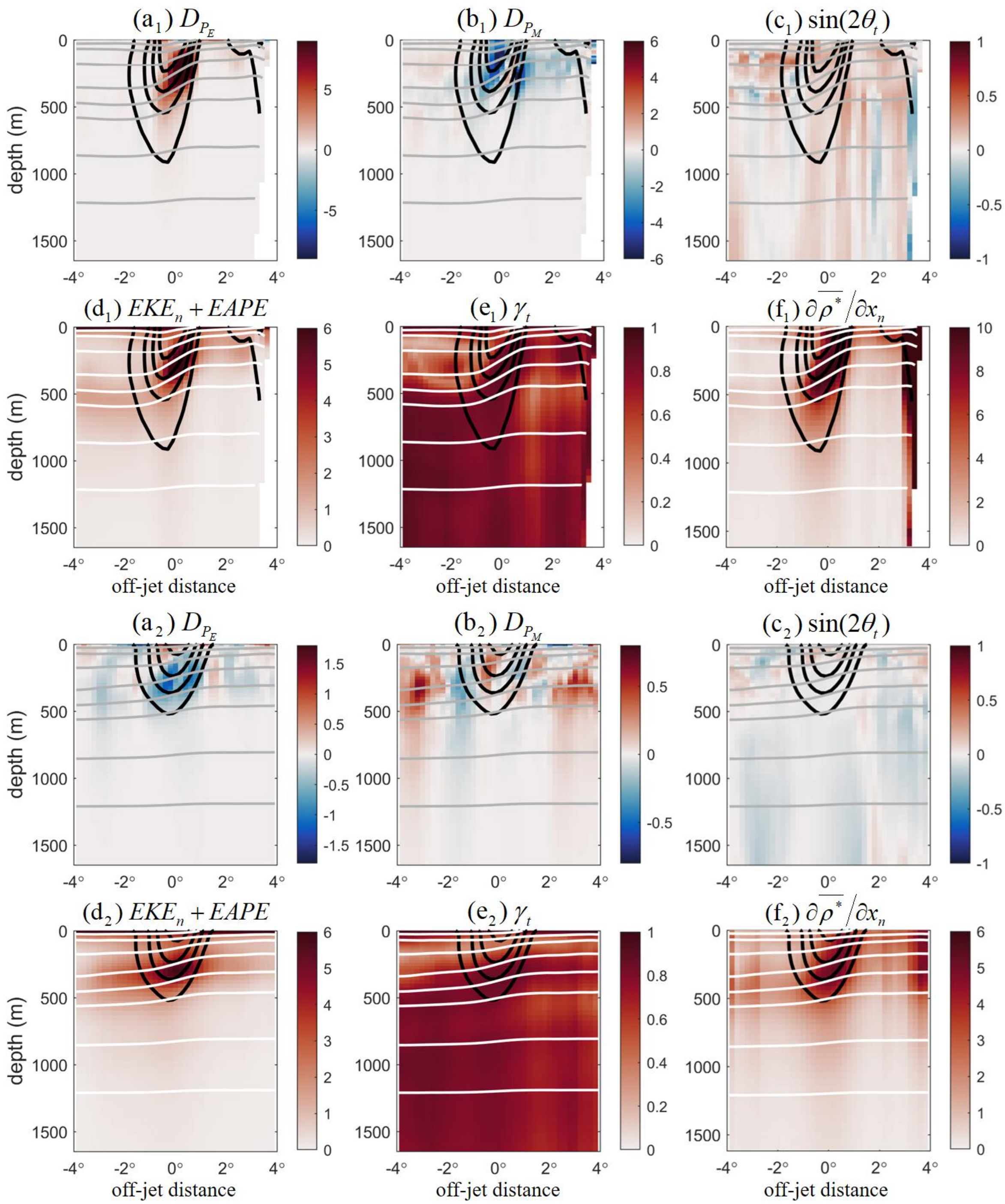

Figure S9. The same as Fig. 14 in the main text, but based on the MITgcm llc4320 solution (2011/09/13-2012/11/14).

Text S4. Statistical test

Text S4a. Bootstrapping technique

In Section 4a of the main text, we estimated the spatial correlation between $|M_{K_{E,geo}} - M_{K_E}|$ and $|\nabla H|$ at each depth, where H denotes the ocean depth. We found that the correlation coefficients are statistically significant at each depth level. The uncertainties of these correlation coefficients are determined using a widely used bootstrapping technique (e.g., Chen et al. 2014b; Chernick, 2011; Schulte et al. 2016; Ivanova et al. 2021). Specifically, we sample the original data for N_{boot} times, randomly selecting a subset of the original data with fixed size N_{sub} each time. Then we estimate a correlation coefficient using each subset with the size N_{sub}. The error bar of the correlation coefficient at 95% confidence level is simply $2\sigma_{boot} \big/ \sqrt{N_{boot}}$, where σ_{boot} represents the standard deviation of all the correlation coefficients obtained using the subsets of the original data. For details of this technique, see Chernick (2011) and the supporting information in Ivanova et al. (2021).

Text S4b. Estimating standard error

Figure 9 in the main text shows the Lorenz energy diagram in the Kuroshio Extension region. The uncertanties of the time-mean energy conversion terms, shown in Fig. 9, were estimated following Chen et al. (2014a). Specifically, the energy conversion term is essentially a time series. Assuming that the time series has M data points and C(n) denotes the autocorrelation of the time series, we can estimate the number of degrees of freedom N from

$$N = M/\max[\sum_{n=-N_0}^{N_0} C(n)].$$

One standard error of the time series, representing uncertainties of the time mean at 65% confidence level, is simply $\sigma/\sqrt{N}$. Here σ is the standard deviation of the time series. The uncertainties shown in Fig. 9 are two standard errors, corresponding to 95% confidence level. For details, see Chen et al. (2014a) and Section 3.6.3 from Chen (2013).

References

Chen, R., 2013. Energy pathways and structures of oceanic eddies from the ECCO2 state estimate and simplified models (Doctoral dissertation, Massachusetts Institute of Technology).

Chen, R., Flierl, G.R. and Wunsch, C., 2014a. A description of local and nonlocal eddy–mean flow interaction in a global eddy-permitting state estimate. Journal of Physical Oceanography, 44(9), pp.2336-2352.

Chen, R., McClean, J.L., Gille, S.T. and Griesel, A., 2014b. Isopycnal eddy diffusivities and critical layers in the Kuroshio Extension from an eddying ocean model. Journal of physical oceanography, 44(8), pp.2191-2211.

Chernick, M.R., 2011. Bootstrap methods: A guide for practitioners and researchers. John Wiley & Sons.

Forget, G. and Wunsch, C., 2007. Estimated global hydrographic variability. Journal of Physical Oceanography, 37(8), pp.1997-2008.

Ivanova, D.P., McClean, J.L., Sprintall, J. and Chen, R., 2021. The Oceanic Barrier Layer in the Eastern Indian Ocean as a Predictor for Rainfall Over Indonesia and Australia. Geophysical Research Letters, 48(22), p.e2021GL094519.

Schulte, J.A., Najjar, R.G. and Li, M., 2016. The influence of climate modes on streamflow in the Mid-Atlantic region of the United States. Journal of Hydrology: Regional Studies, 5, pp.80-99.